Hydrothermal fluid flow within a tectonically active rift-ridge transform junction: Tjornes Fracture Zone, Iceland

JOURNAL OF GEOPHYSICAL RESEARCH, VOL. 115, B05104, doi:10.1029/2009JB006640, 2010

Hydrothermal fluid flow within a tectonically active rift-ridge transform junction: Tjörnes Fracture Zone, Iceland

M. Lupi,[1] S. Geiger,[1] and C. M. Graham[2]

Received 22 May 2009; revised 30 November 2009; accepted 18 December 2009; published 26 May 2010.

[1] We investigate the regional fluid flow dynamics in a highly faulted transform area, the Tjörnes Fracture Zone in northern Iceland which is characterized by steep geothermal gradients, hydrothermal activity, and strong seismicity. We simulate fluid flow within the Tjörnes Fracture Zone using a high-resolution model that was based on the available geological and geophysical data and has the aim to represent the complex geological structures and the thermodynamical processes that drive the regional fluid flow in a physically realistic way. Our results show that convective heat flow and mixing of cold and saline seawater with deep hydrothermal fluids controls the large-scale fluid flow. The distribution of faults has a strong influence on the local hydrodynamics by focusing flow around clusters of faults. This explains the nature of isolated upflow zones of hot hydrothermal fluids which are observed in the Tjörnes Fracture Zone. An important emergent characteristic of the regional fluid flow in the Tjörnes Fracture Zone are two separate flow systems: one in the sedimentary basins, comprising more vigorous convection, and one in the crystalline basement, which is dominated by conduction. These two flow systems yield fundamental insight into the connection between regional hydrothermal fluid flow and seismicity because they form the basis of a toggle switch mechanism that is thought to have caused the hydrogeochemical anomalies recorded at Húsavik before and after the 5.8 M earthquake in September 2002.

Citation: Lupi, M., S. Geiger, and C. M. Graham (2010), Hydrothermal fluid flow within a tectonically active rift-ridge transform junction: Tjörnes Fracture Zone, Iceland, *J. Geophys. Res.*, *115*, B05104, doi:10.1029/2009JB006640.

1. Introduction

[2] Iceland is a geologically young and volcanically active region. Its formation is connected to the seafloor spreading processes which separate the North American and European plates. The Mid-Atlantic Ridge cuts through Iceland, creating a unique geologic scenario (Figure 1a). Rock ages range from late Tertiary (in the western, eastern and northern fjords) to recent times. The latter can be found in the central active volcanic belts, where the Mid-Atlantic Ridge crops out [*Jóhannesson and Sæmundsson*, 1998]. Iceland's young crust is still warm and volcanic activity, intense seismicity and large hydrothermal fields are abundant [*Palmason and Sæmundsson*, 1974; *Sæmundsson*, 1979; *Arnórsson*, 1995a, 1995b]. The study of fluid flow in hydrothermal systems has a long history in Iceland because geothermal energy is plentiful [*Flóvenz*, 2008]. Consequently, major research efforts focus on understanding heat transfer and phase distribution in geothermal fields that are currently used for providing Iceland with energy [e.g., *Bodvarsson et al.*, 1984a, 1984b, 1984c]. However, there is also long-standing, more scientific interest in investigating the interaction between fluid flow and magmatic intrusions [c.f., *Lowell*, 1991; *Driesner and Geiger*, 2007; *Ingebritsen et al.*, 2010] for which Iceland provides an excellent natural laboratory.

[3] Recently it was demonstrated that there is a strong coupling between regional fluid flow dynamics and seismic events in magmatic hydrothermal systems [*Manga and Brodsky*, 2006]. This is documented by rapid postseismic changes in black-smoker vent temperatures [*Johnson et al.*, 2000], variations in geyser periodicity [*Husen et al.*, 2004] and water level changes in deep wells [*Hill et al.*, 1993; *Roeloffs et al.*, 2003].

[4] In northern Iceland, variations in the hydrogeochemistry of ice age waters were detected at Húsavik before and after a 5.8 M earthquake [*Claesson et al.*, 2004, 2007]. The town of Húsavik is located in the Tjörnes Fracture Zone (TFZ) (Figure 1b), which is the highly tectonized transform area that connects the rift segments of the Mid-Atlantic Ridge. Several faults, grabens and sedimentary layers characterize this seismically active region [*Sæmundsson*, 1974; *Gudmundsson et al.*, 1993; *Rögnvaldasson et al.*, 1998; *Gunnarsson*, 1998; *Gudmundsson*, 2007]. In addition to tectonically induced

[1]Institute of Petroleum Engineering, Heriot-Watt University, Edinburgh, UK.
[2]School of Geosciences, University of Edinburgh, Edinburgh, UK.

0148-0227/10/2009JB006640

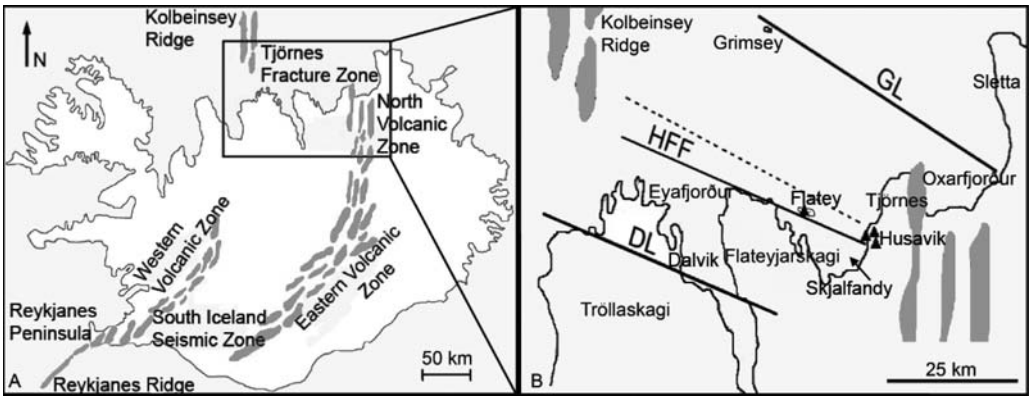

Figure 1. (a) Map of Iceland showing the Mid-Atlantic Ridge and the most important volcanically and tectonically active regions. (b) Close up of the Tjörnes Fracture Zone. The black bold lines represent the Grimsey Lineament (GL), the Húsavik Flatey Fault (HFF), and the Dalvik Lineament (DL). The dotted line represents the trace of the seismic line from which we reconstructed the two-dimensional geological model for the numerical simulations. The black triangles are the locations of the boreholes and include the borehole "Húsavik-Hola nr. 1", where hydrogeochemical variations before and after a 5.8 M earthquake were observed [*Claesson et al.*, 2004, 2007].

earthquakes, two further types of seismic events occur in this area: dike-induced and hydrothermally induced earthquakes [*Hensch et al.*, 2007]. *Claesson et al.* [2004, 2007] suggested that the chemical variations observed at Húsavik are caused by a "toggle switch" mechanism in permeability [*Miller and Nur*, 2000]: the permeability of a fault increases instantaneously during a seismic event and decreases slowly during the postseismic period when minerals precipitate and the effective normal stress on the fault changes. During the seismic event at Húsavik, the permeability increase of a fault is thought to connect two reservoirs containing fluids of different chemical signature. Fluids from one reservoir are then transported upwards from great depth along the fault into the second reservoir, causing the instantaneous change in hydrogeochemistry observed at Húsavik. When the fault permeability decays, the communication between the two reservoirs decreases, causing the gradual change in hydrogeochemistry observed at Húsavik. Although chemical, seismic, and geophysical data indicate a strong connection between hydrothermal fluid flow and seismicity in the TFZ [*Claesson et al.*, 2004, 2007; *Hensch et al.*, 2007; *Stefansson et al.*, 2008], a regional fluid flow model that explains how these processes in the TFZ are fundamentally interlinked does not yet exist.

[5] The objective of this study is hence to develop a dynamic fluid flow model for the TFZ that we base on high-resolution simulations. These simulations account for the geological complexity of the TFZ and the physical complexity of hydrothermal fluids. With the help of this flow model we aim to answer the following five questions: (1) What is the link between large-scale hydrothermal fluid flow and seismicity in the TFZ? (2) Is the proposed toggle switch mechanism for the TFZ possible and where could it occur? (3) How do the abundant faults in the TFZ influence fluid flow and what is their role in linking hydrothermal fluid flow and seismicity? (4) Can we identify the key parameters that control the large-scale flow behavior? (5) What is the nature and the origin of the low-temperature hydrothermal fluids in the TFZ?

[6] Traditionally, new insights into the hydrodynamics of hydrothermal systems were gained by "process models" which tend to idealize the geological structures and instead focus on a more detailed description of the physical processes [e.g., *Cathles*, 1977; *Hanson*, 1995; *Hayba and Ingebritsen*, 1997; *Wilcock*, 1998; *Garven et al.*, 2001; *Hurwitz et al.*, 2003; *Fisher et al.*, 2003; *Join et al.*, 2005; *Fontaine et al.*, 2007; *Lowell et al.*, 2007; *Coumou et al.*, 2008]. However, given today's computational power and progress in numerical algorithms for modeling hydrothermal systems [*Ingebritsen et al.*, 2010], our aim was to develop a dynamic flow model that accounts for both physical complexity and geological detail. This approach is still little used but offers a tremendous upside because it allows us to reveal the hidden, i.e. emergent, properties of a hydrothermal system while specifically considering a geological model that incorporates the key structures observed in nature [*Matthäi et al.*, 2004]. We hence constructed a detailed two-dimensional geological model along a seismic cross section using the available geological, geophysical and borehole data for the TFZ. This model accounts for the faults, the unconformities and the lateral discontinuities which characterize the geology of the TFZ. We then employed the code "Complex System Modeling Platform – CSMP++" [*Matthäi et al.*, 2007], a state-of-the-art simulator for modeling fluid flow in structurally complex reservoirs, to simulate the transient evolution of fluid flow in this geological model using representative boundary conditions for the TFZ. We also used a more realistic thermodynamic description for binary hydrothermal fluids containing NaCl and H_2O [*Driesner and Heinrich*, 2007; *Driesner*, 2007] because salt (NaCl) is the most abundant chemical component in hydrothermal fluids. It has profound effects on the thermodynamics and hydrodynamics [*Geiger et al.*, 2005; *Coumou et al.*, 2009]. Although the most important thermodynamic effect is that NaCl-H_2O fluids can boil and separate into a high-density brine and low-density vapor at temperatures and pressures much above the critical point of pure water and two fluid phases can flow simultaneously under certain pressure,

temperature, and salinity conditions, these processes are not common in the Tjörnes Fracture Zone or at least in our simulations. Complex hydrodynamic systems can also evolve because salt and heat diffuse and advect at different rates, providing competing effects that try to stabilize or trigger hydrothermal convection. These thermodynamic and hydrodynamic effects cannot be captured if the fluid is assumed to be pure water.

[7] The paper is organized as follows: in section 2 we present the geological model of the TFZ. This is followed by a description of the model setup, including its hydraulic properties, boundary, and initial conditions. Then we discuss the mathematical model and the numerical methods. Finally, we describe the results and explain how they relate to available geological data. From this we develop a regional flow model for the Tjörnes Fracture Zone which describes the "interseismic" state, i.e. the hydrodynamic state between earthquakes, and discuss how this state may be altered by earthquakes in a toggle switch process.

2. Geological Setting

[8] The Tjörnes Fracture Zone is the region located between the Slétta peninsula and the Kolbeinsey Ridge (Figure 1). It is the geological expression of the rifting processes taking place in the north Iceland. The offset of the axial rifting zone is around 100 km along the TFZ and the overall geological setting is characterized by complex tectonics. Several north trending, subsiding troughs and volcanic chains occur in the area [*Sæmundsson*, 1974] as well as NW-SE trending strike-slip faults and grabens [*Rögnvaldasson et al.*, 1998]. The strong seismicity which occurs in this region is continuously monitored by the Icelandic Meteorological Office. Since 1994, a consistent seismic station network has been installed in north Iceland as part of the south Iceland lowland system [*Jakobsdóttir et al.*, 2002]. The seismic events are induced by tectonic activity, hydrothermal fluid circulation, and dike intrusions at depth [*Hensch et al.*, 2007]. The thickness of the highly tectonized crust decreases from east to west: close to the North Volcanic Zone it is ~26 km thick, in the vicinity of Grimsey Island it decreases to 16 km and reaches a minimum of 7 km close to the Kolbeinsey Ridge [*Riedel et al.*, 2005].

[9] The main tectonic structures in this region, the Grimsey lineament, the Húsavik Flatey Fault and the Dalvik lineament, are defined by abundant microseismicity [*Stefansson et al.*, 2008]. The Grimsey lineament and the Dalvik lineament form the boundaries of the TFZ. The on-land expression of the Grimsey lineament is hardly visible but offshore it is clearly identifiable by seismicity. The microearthquake epicenters define a lineament trending about N52°W with right-lateral strike-slip faulting [*Stefansson et al.*, 2008]. The Grimsey lineament has been seismically active at least since 1967. It is strongly connected to the North Volcanic Zone as shown by the occurrence of a seismic swarm which preceded the volcanotectonic episode at Krafla in 1975 [*Gudmundsson et al.*, 1993].

[10] The Húsavik Flatey Fault is a dextral transform fault and a key tectonic feature of the TFZ. It has a right-lateral displacement between 5 and 10 km. The fault mainly runs offshore and its displacement may reach a maximum of 60 km [*Sæmundsson*, 1974]. On land it joins the north trending normal faults of the Þeistareykir fissure swarm [*Gudmundsson et al.*, 1993]. From borehole data it has been estimated that the maximum vertical displacement is approximately 1.4 km [*Tryggvason*, 1973]. The Húsavik Flatey Fault crops out on the Flateyjarskagi Peninsula at the western end of the TFZ. Here a 3 to 5 km wide damaged zone, characterized by small-scale strike-slip faults, transform-parallel trending fault cores of completely crushed rocks and extensive mineral vein patterns, is visible [*Gudmundsson*, 2007]. Offshore the fault flanks the Flateyjarskagi peninsula (parallel to a 3 to 4 km deep graben) and almost reaches the Kolbeinsey Ridge at the eastern end of the TFZ. Most of the seismic activity is concentrated close to the Kolbeinsey ridge and between the mouth of the Eyafjordur and the Flatey shelf [*Hensch et al.*, 2007].

[11] The Dalvik lineament lies subparallel to the Húsavik Flatey Fault and runs close to the town of Dalvik, as shown by the consistent seismic activity which begins almost 30 km south of Húsavik. Usually the seismicity is localized offshore in the western part, although a strong earthquake swarm occurred in 1934 close to the town of Dalvik. It has been proposed that these seismic events were related to a strike-slip fault with a right-lateral strike-slip movement [*Sykes*, 1967; *Einarsson*, 1976].

[12] Although the most abundant earthquakes are associated with these three geological structures, it is important to note that large earthquakes with a magnitude above four can also occur away from them, that is in the center of the TFZ [*Stefansson et al.*, 2008].

[13] At least three well-defined sedimentary basins overlaying the oceanic crust can be identified in the TFZ [*Gunnarsson*, 1998] (Figure 1b): the Öxarfjordur graben, the Skjálfandi graben and the Eyjafjar aráll graben. Their formation has been related to the extensional tectonic regime which started in the late Miocene and is still active today [*Gudmundsson*, 2007]. The origin of the basin infill is linked to the high erosion rate of the Icelandic glaciers during the Pleistocene. They probably have produced sediments that are coarser than typical marine sediments [*Gunnarsson*, 1998]. Data from the borehole Húsavik-Hola nr. 1, near the town of Húsavik, show sandstones intercalated with gravels and interlayered with lavas at a depth of 1.4 km [*Tomasson et al.*, 1969]. This provides a partial reference for the lithology of the seismic cross section used to construct our geological model.

[14] The sedimentary basins reach a depth of ~4 km. Below, picritic rocks occur up to 5 km depth. Gabbros, which characterize the lower oceanic crust, reach a depth between 10 km and 20 km [*Riedel et al.*, 2005]. The seismic velocity structure of the TFZ shows an increase in P wave and S wave velocities at 4 km depth (below the top of the crystalline basement) [*Riedel et al.*, 2005]. This might be a consequence of the closing of cracks which reduces the percolation of water and subsequently causes less hydrothermal alteration of the rocks [*Riedel et al.*, 2005]. Below the gabbroic bodies a MgO rich mantle is present [*Riedel et al.*, 2005].

3. Numerical Simulations

[15] We used multichannel seismic reflection data that were recorded in the Tjörnes Fracture Zone by the Icelandic

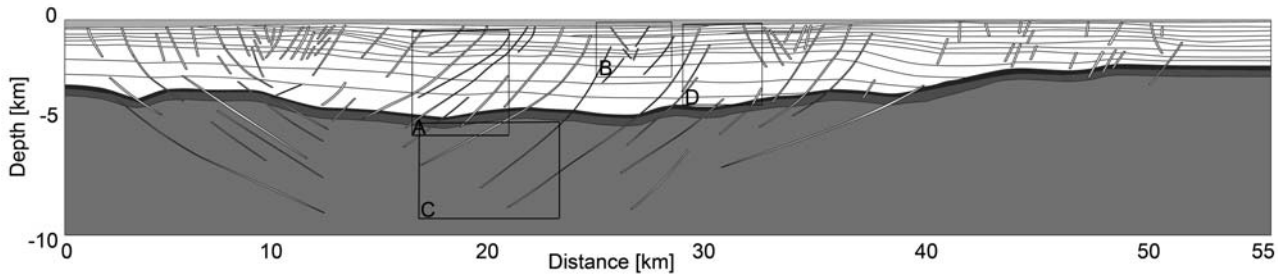

Figure 2. Geometry of the geological structures (i.e., faults, sedimentary layers, and crystalline basement) which comprise the hydrostratigraphic units of the two-dimensional model used in the numerical simulations. The hydraulic and petrophysical properties of the units are listed in Table 1. The light grey region at the top represents the sea (note the irregular seafloor topography). The dark grey region in the center is the top of the crystalline basement, the medium grey region is the shallow basement, and the light grey region the deep basement. Insets A to C show the locations of the flow fields depicted in Figure 7. Inset D shows the location of the sedimentary layers depicted in Figure 3.

National Energy Authority [*Gunnarsson*, 1998] as the basis for our two-dimensional geological model. The NW-SE trending seismic profile is shown in Figure 1. It runs parallel to the Húsavik Flatey Fault and terminates close to the town of Húsavik. It cuts the main sedimentary basins and NE-SW trending faults of the TFZ but not the Grimsey lineament, the Húsavik Flatey Fault, or the Dalvik lineament. There are two reasons for selecting this particular seismic line as the basis for our geological model. First, we wanted to simulate fluid flow in the center of the TFZ where large-magnitude earthquakes can occur. This seismic line is located comparatively central in the TFZ. Secondly, of the different seismic lines recorded by the Icelandic National Energy Authority [*Gunnarsson*, 1998] and other seismic profiles of the TFZ [*Riedel et al.*, 2005], this line has the best quality and also resolves a large number of faults and shallower sedimentary layers. Furthermore, it is located in the vicinity of boreholes (Figure 1) which provide temperature measurements at depth and some indication as to how the shallow sedimentary layers could correlate to the stratigraphy of the TFZ.

3.1. Geometric Modeling

[16] Translating a geometrically complex environment like the TFZ into a computational grid that can be used for numerical simulations is challenging. We first reconstructed the geometry of the geological structures identified in our two-dimensional seismic cross section [*Gunnarsson*, 1998] using the CAD software Rhinoceros 4.0™ [*Paluszny et al.*, 2007]. We then discretised the resulting CAD geometry into approximately 50,000 adaptively refined triangular finite elements using the commercial software ANSYS ICEM™.

[17] The resulting numerical model includes 86 faults, classified as shallow and deep (Figures 2 and 3). They link the upper and the lower structural levels of the system. The shallow faults reach a maximum depth of 1 km while the deep faults start at 1 km and reach depths of 9 km. We discretised each fault by triangular finite elements such that the area of the finite elements is approximately equal to half the width of the fault squared. The finite element grid is hence significantly refined around the faults. Although field data suggest that the faults are structurally complex and consist of a high-permeability damaged zone and low-permeability fault core [*Evans et al.*, 1997; *Gudmundsson*, 2001, 2007], we only reproduce the damaged zone in our model and represent the faults as discrete structures ranging from 120 m to 20 m in width. We also tested the influence of a low-permeability fault core on hydrothermal flow patterns. Fluid flow in the TFZ, however, is predominantly parallel to the subvertical faults due to large-scale convection. Hence it is not influenced much by the low-permeability fault core, which would only be of importance if flow were predominantly horizontal (i.e., across the faults). By not discretising the fault cores of the individual faults, we were able to speed up our simulations by a factor of 10 to 100. The discretisation of the very narrow fault core would require a very large number of excessively small finite elements. These small elements would require a significant reduction in the size of the time step, which is directly proportional to the area of a finite element and the flow velocity in it.

[18] We divided the crystalline basement into three parts (top, shallow and deep basement) to reproduce the geology shown by other seismic profiles of the TFZ [*Riedel et al.*,

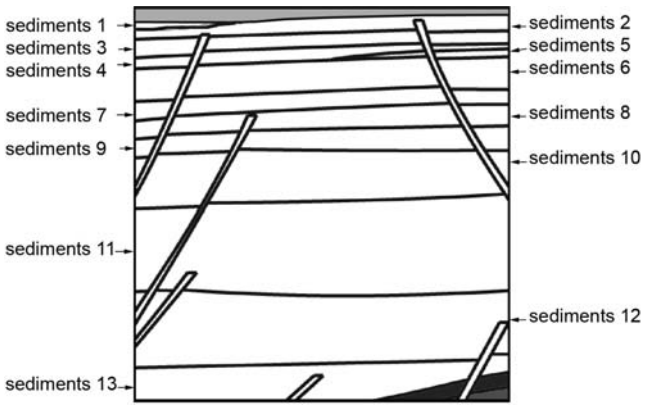

Figure 3. Closeup of Figure 2 showing the sedimentary layers, which have been correlated from the seismic cross section and form the hydrostratigraphic units of the sedimentary basin. The hydraulic properties of the layers are listed in Table 1.

Table 1. Values of the Permeability, Porosity, Heat Capacity, and Density for All Hydrostratigraphic Units Which Comprise the Hydrostatigraphy of the TFZ[a]

Group	$\log(k)$ (m^2)	ϕ (−)	c_{pr} (J/(kg m))	ρ_r (kg/m^3)
Sediments 1	−13	0.25	1000	2700
Sediments 2	−13	0.25	1000	2700
Sediments 3	−14	0.20	1000	2700
Sediments 4	−14	0.20	1000	2700
Sediments 5	−15	0.15	1000	2700
Sediments 6	−15	0.15	1000	2700
Sediments 7	−15	0.15	1000	2700
Sediments 8	−16	0.15	900	2600
Sediments 9	−16	0.10	1200	2900
Sediments 10	−15	0.10	1000	2600
Sediments 11	−15	0.10	1000	2700
Sediments 12	−15	0.10	1000	2600
Sediments 13	−15	0.15	1100	2600
Shallow faults	−13.5	0.22	1100	2800
Group	$\log(k_0)$ (m^2)	ϕ (−)	c_{pr} (J/(kg m))	ρ_r (kg/m^3)
Deep faults	−13.70	0.02	1200	2800
Top basement	−13.75	0.02	1200	3000
Shallow basement	−13.90	0.02	1200	3200
Deep basement	−14.00	0.02	1200	3200

[a]See Figures 2 and 3 for their locations. The thermal conductivity and compressibility of all units is constant at 2.5 W m^{-1} $°C^{-1}$ and 10^{-12} Pa^{-1}, respectively. The dispersion tensor is isotropic and 10^{-6} m^2 s^{-1} in the sedimentary basins and 10^{-9} m^2 s^{-1} in the crystalline basement. $\log(k_0)$ denotes that the permeability of this unit varies as a function of depth according to equation (1) and is the permeability at 1 km depth.

2005]. The top basement, ~100 m thick, is assumed to be strongly hydrothermally altered and characterized by frequent occurrence of joints and fractures. The shallow basement (between ~100 and ~600 m below the sediments) is characterized by permeabilities which guarantee the percolation of fluids at these depths [*Riedel et al.*, 2005]. The deeper parts of the basement are probably of gabbroic origin [*Riedel et al.*, 2005] and assumed to have low permeability.

3.2. Geological Characterization of the Model and Petrophysical Parameters

[19] Our geological model of the TFZ contains 18 lithological units, which comprise the hydrostratigraphy (Figures 2 and 3). Each hydrostratigraphic unit is equipped with a unique set of hydraulic and petrophysical parameters, i.e. permeability k, porosity ϕ, density ρ_r, thermal conductivity K, heat capacity c_{pr}, and compressibility β_r. The subscript r denotes the rock. Each unit is listed in Table 1 along with its porosity, permeability, density, and heat capacity. The thermal conductivity of all units is held constant at 2.5 W m^{-1} $°C^{-1}$. However, the thermal diffusivity of the different rock types κ, defined as $\kappa = K/(\rho_r c_{pr})$, can still vary due to the local variations in density and heat capacity. The compressibility of all units is also held constant at 10^{-12} Pa^{-1}. However, the bulk compressibility of the fluid-saturated rock is dominated by the fluid compressibility, which varies with temperature and pressure. Dispersion of salt is described by an isotropic dispersion tensor, which is 10^{-6} m^2 s^{-1} in the sedimentary basins and 10^{-9} m^2 s^{-1} in the crystalline basement.

[20] All hydraulic and petrophysical properties are constant in each unit over space and time with the exception of the permeability of the deep faults and crystalline basement. Here the permeability varies as a function of depth according to the relationship provided by [*Manning and Ingebritsen*, 1999]

$$\log(k) = \log(k_0) - 3.2 \cdot \log(z), \quad (1)$$

where $\log(k_0)$ is the permeability that the layer would have at 1 km depth and z denotes the depth in kilometers. *Manning and Ingebritsen* [1999] used $\log(k_0) = -14$ m^2.

[21] A closeup of the sedimentary basins and the layering of the shallow crust is shown in Figure 3. The sedimentary units are classified according to depth (Table 1): "sediments 1" are closest to the seafloor while "sediments 13" are situated just above the crystalline basement. The porosity and permeability (denoted as ϕ and k in Table 1, respectively) of the sedimentary units are assigned such that they generally decrease from top to bottom of the basins, mimicking the increased compaction of the oldest and deepest sediments. The porosity of the deep faults is assumed to be low due to the precipitation of mineral phases into the pore space. The basement and deep faults (i.e., below 1 km depth) have depth-dependent permeabilities. The corresponding values for $\log(k_0)$ (equation (1)) are listed in Table 1. The shallow faults (between 0 to 1 km depth) have constant permeabilities.

3.3. Key Assumptions

[22] We have made several assumptions and simplifications with respect to the numerical simulation. These were practical decisions driven by the necessity to keep the computational cost reasonable.

[23] The mathematical formulation used in this study does not account for two-phase flow and the dynamic formation of a brine and vapor phase. However, in the numerical implementation we checked for each time step if pressure, temperature, and salinity conditions could lead to the formation of brine and vapor. In this case the simulation is terminated automatically because the mathematical model is inadequate for this physical processes. Over the many simulations ran in this study we rarely encountered this situation. This is because the downwelling of cold, saline seawater continuously cools the hydrothermal system, depressing the geothermal gradient and avoiding boiling, particularly at shallower depths. Supercritical transition from brine-like to vapor-like fluids, as it can occur at great depth in the TFZ, is still modeled correctly by the equations.

[24] We assumed that all hydraulic and petrophysical properties are constant with time. The decrease (or the enhancement) of properties like permeability and porosity due to external factors (e.g., changes in regional stress, creation of new faults during the extension of the TFZ, mineral precipitation or dissolution) are not accounted for. Including the transient evolution of permeability and porosity into the numerical simulations will add another level of complexity and uncertainty because models to describe these processes are not well constrained.

[25] We also assumed that the boundary conditions are constant through time. This neglects, for example, any changes in heat flow due to changes in magmatic activity or changes in seafloor topography due to sediment deposition.

[26] Our simulations account only for two-dimensional geometries. This implies that convection in the fault plane,

which is likely to occur during hydrothermally driven fluid flow and may be affected by regional groundwater flow [*Bächler et al.*, 2003], is neglected. A three-dimensional flow model of the TFZ would require a significant simplification of the geological structures to keep computational costs reasonable. It would also add another level of uncertainty. Due to the scarcity of three-dimensional seismic data and lack of constraints on regional groundwater flow in the TFZ, it is unknown how far the faults extend in the third dimension and how regional groundwater flow, particularly in the faults, could affect hydrothermal flow patterns locally. Our aim was to study the transient evolution of fluid flow in a geologically realistic representation and try to identify the key parameters controlling the large-scale fluid flow. Given the geological complexity of the TFZ, the insights from a detailed two-dimensional model are still significant.

3.4. Boundary and Initial Conditions

[27] All simulations were run for ~1 Ma. This provides enough time for the flow system to evolve but is well below the age of the TFZ, which is 6 to 7 Ma [*Gunnarsson*, 1998], such that we can assume that many of the geological structures along our two-dimensional cross section are already in place.

3.4.1. Top, Left, and Right Boundary

[28] The hydrostatic pressure in the sea above the TFZ varies along the seafloor according to the water depth given by the seafloor morphology. We used the hydrostatic pressure at the seafloor as the boundary condition for the fluid pressure. We assumed that the temperature of the seawater at the seafloor is 5°C and used a uniform seawater salinity of 3.2 Wt.% NaCl. We applied these values as uniform boundary conditions for temperature and salinity, respectively, at the seafloor. We kept the boundary conditions for pressure, temperature, and salinity constant during the simulation. The left, right, and basal boundaries are no-flow boundaries.

3.4.2. Heat Flow at the Basal Boundary

[29] We applied a constant heat flow rate at the base of the model. Data from *Flóvenz and Sæmundsson* [1993] indicate a heat flow rate of 0.15 W m^{-2} close to the city of Húsavik and lower rate of 0.10 W m^{-2} in the Tjörnes Fracture Zone. *Flóvenz et al.* [1985] and *Flóvenz* [2008] propose geothermal gradients of 50 to 60°C km^{-1} for the sedimentary basins of the TFZ. Picritic rocks at shallow depths suggest a very hot upper mantle [*Riedel et al.*, 2005] and *Stefansson et al.* [2008] infer partially molten basalts at 10 to 15 km depth in the TFZ. This could imply higher heat flow rates than originally suggested by *Flóvenz and Sæmundsson* [1993]. Most of our simulations used a heat flow rate of 0.18 W m^{-2}. Since the heat flow rate applied to the basal boundary will have a major impact on the geothermal gradient and on the flow dynamics, we ran additional simulations to test the effects caused of lower heat flow rates of 0.15 W m^{-2} and 0.10 W m^{-2}.

3.4.3. Initial Conditions

[30] We computed the initial geothermal gradient and hydrostatic pressure, as well as the initial distribution of fluid properties (i.e., viscosity, density, heat capacity), iteratively using the boundary conditions for pressure and temperature discussed above. For this we solved equations (5) and (4) at steady state, i.e. with $\partial T/\partial t = \partial p/\partial t = 0$, and updated the fluid properties during each iteration using an equation of state for NaCl-H_2O [*Driesner and Heinrich*, 2007; *Driesner*, 2007]. Note that we assume an undisturbed initial hydrostatic fluid pressure and hence set the fluid velocities in equation (5) to zero during the calculation of the initial geothermal gradient. These calculations imply if the heat flow rate at the basal boundary is changed, the initial geothermal gradient will be different and with that the initial hydrostatic fluid pressure because the fluid density is a function of temperature. The initial salinity was always set to zero in the crust.

3.5. Mathematical Formulation

[31] We used the mathematical model for NaCl-H_2O fluid flow developed by *Geiger et al.* [2006a] and modified by *Coumou et al.* [2009]. Salt (NaCl) is the most abundant chemical component in hydrothermal fluids and has profound effects on their thermodynamics [*Driesner and Heinrich*, 2007; *Driesner*, 2007] and hydrodynamics [*Geiger et al.*, 2005; *Coumou et al.*, 2009]. Mass conservation of a NaCl-rich fluid is given by

$$\phi \frac{\partial \rho_f}{\partial t} = -\nabla \cdot \left(\mathbf{v_f} \rho_f\right), \tag{2}$$

where ϕ is the porosity, ρ_f the fluid density and $\mathbf{v_f}$ the Darcy velocity. Note that here and in the following we neglect source/sink terms for simplicity.

[32] Momentum conservation is given by Darcy's law [*Ingebritsen and Sanford*, 2006]

$$\mathbf{v_f} = -\frac{k}{\mu_f}\left[\nabla p - \rho_f \mathbf{g}\right], \tag{3}$$

where k is the permeability (here assumed to be a scalar), μ_f the fluid viscosity, p the fluid pressure and $\mathbf{g}$ the vector of gravitational acceleration. Darcy's law and the mass conservation equation can be combined to formulate a pressure diffusion equation

$$\rho_f \beta_t \frac{\partial p}{\partial t} = \nabla \cdot \left[\left(\frac{k}{\mu_f}\rho_f\right)\nabla p\right] - \nabla \cdot \left[\frac{k}{\mu_f}\rho_f^2 \mathbf{g}\right] + \rho_f \phi \left[\gamma_f \frac{\partial X}{\partial t} - \alpha_f \frac{\partial T}{\partial t}\right]. \tag{4}$$

Here, α_f and γ_f are the thermal expansivity and the chemical expansivity, respectively. β_t is the total compressibility of the fluid and rock, given by $\beta_t = (1 - \phi)\beta_r + \phi\beta_f$. The subscripts r and f denote the rock and the fluid, respectively.

[33] Conservation of energy can be approximated as

$$\left[(1-\phi)\rho_r c_{pr} + \phi\left(\rho_f c_{pf}\right)\right]\frac{\partial T}{\partial t} = -\nabla \cdot \left(\mathbf{v_f} c_{pf} \rho_f T\right) + \nabla \cdot (K \nabla T), \tag{5}$$

where c_{pf} is the isobaric heat capacity and K is the thermal bulk conductivity of fluid and rock.

[34] Mass conservation of NaCl is given by

$$\phi \frac{\partial (\rho_f X_f)}{\partial t} = -\nabla \cdot \left(\mathbf{v_f} \rho_f X_f\right) + \nabla \cdot \left(\mathbf{D} \nabla \rho_f X_f\right), \tag{6}$$

where **D** is the dispersion tensor, which we assume to be isotropic and symmetric. X_f is the mass fraction NaCl.

3.6. Numerical Solution

[35] The numerical model was implemented in the "Complex System Modeling Platform – CSMP++" [*Matthäi et al.*, 2007]. We solved the governing equations by a combination of finite element and finite volume methods [*Geiger et al.*, 2006a, 2006b]. The finite element method approximates the diffusive parts of the governing equations while the finite volume method approximates the advective parts. The advective parts were solved explicitly using a higher-order flux approximation [*Geiger et al.*, 2004]. The diffusive parts were solved implicitly, using an algebraic multigrid solver to invert the resulting system of linear equations [*Stüben*, 2001].

[36] The governing equations were linearized by decoupling the pressure equation (equation (4)) from the energy and solute conservation equations (equations (5) and (6)) [*Geiger et al.*, 2006a, 2006b]. They can then be solved sequentially for each time step in five steps. First the diffusion of temperature and salinity is calculated with the finite element method and implicit time stepping. Next, the advection of temperature and salinity is computed by using the finite volume method and explicit time stepping. Afterwards the fluid properties are updated and the diffusion of the fluid pressure is computed by the finite element method and implicit time stepping. Finally the velocity field is updated. The size of the time increment was computed during each time step. It is directly proportional to the smallest ratio of the area of a finite element and the flow rate in the finite element. Hence the time step is adapted automatically as the flow rates in the model increase or decrease. This allows us to resolve changes in the transport processes at the rate at which they occur.

[37] During each time step the fluid properties μ_f, ρ_f, and c_{pf}, and their derivatives β_f, α_f and γ_f, needed for the solution of equations (2)–(6), were directly computed from an equation of state for NaCl-H_2O for the given temperature, pressure, and salinity field. The equation of state is valid from 0°C to 1000°C, 1 bar to 5000 bar, and 0 to 100 wt % NaCl [*Driesner and Heinrich*, 2007; *Driesner*, 2007].

4. Results

4.1. General Flow Patterns

[38] Figures 4 and 5 show the evolution of the temperature field and flow rates over a time window of 1 Ma. Figure 6 shows the temperature field after 0.9 Ma with its horizontal average removed. The heat flow rate was set to 0.18 W m^{-2} in this simulation. Figure 7 depicts the flow field in selected regions of the geological model (see Figure 2 for their locations). The simulations show the occurrence of two separate flow systems in the Tjörnes Fracture Zone. The first is located in the sedimentary basins and is characterized by comparatively vigorous convection. The second occurs in the crystalline basement where fluids convect at much lower rates. These two flow systems are also expressed by a distinct change in the geothermal gradient. In the shallow sedimentary basins the average geothermal gradient is ~40°C km^{-1} while it is between 90°C km^{-1} and 100°C km^{-1} in the basement. Fluid communication between the two flow systems is limited. The downwelling of fluids from the sedimentary basins into the crystalline basement is limited and occurs mostly along faults. Migration of fluids from the basement to higher structural levels occurs only in regions where zones of hot upwelling fluids are located.

[39] Zones of hot upwelling fluids develop in the sedimentary basins and rise from the top of the basement and reach shallow depths (less than 800 m deep) during the early stages of the system's evolution (Figure 4a). Downwelling and upwelling areas are clearly separated and recognizable through the entire vertical profile of the TFZ. The upflow zones comprise temperatures that are up to 170°C hotter than the average horizontal temperatures while temperature of the downflow areas are approximately 60°C colder than the average horizontal temperature (Figure 6).

[40] After ~0.1 Ma, at least six upflow zones have formed, most of which are up to 4 to 5 km wide. Their locations are not constant. Some plumes merge such that the number of upflow zones decreases with time. For example the central plume of Figure 4a (located between 20 and 30 km) continuously moves from west to east, by approximately 5 km in 0.9 Ma (i.e., less than 1 cm/yr). This lateral migration is also visible in the horizontal temperature and velocity profiles (Figure 5). The lateral migration seems to be mainly controlled by the morphology of the crystalline basement and by the clusters of high permeability faults (Figure 7). After 0.8 Ma, the upflow zones are still migrating slowly in the crust and the system does not reach a steady state despite the presence of permeable faults which can act as main flow conduits and stabilize fluid flow. Since we do not account for changes in permeability or the formation of new faults during extension of the TFZ, we can speculate that the flow system will never reach a true steady state. High salinity fluids, originally located at higher structural levels, reach the deepest parts of the crystalline basement after 0.35 Ma. At this time the salinity of the system is relatively uniform (3.2 Wt %) for the entire crust. Fluids percolate downward slightly faster in the faults, reaching 9 km depth in the early stages of the simulations (~0.15 Ma).

[41] The hydrothermal upflow zones concentrate around clusters of faults (Figures 4 and 7a). They are characterized by flow rates that can be more than one order of magnitude higher compared to the background flow rates in the basement and sedimentary basin (Figure 5). The elevated flow rates in the vicinity of the faults transport hot fluids upwards and consequently the temperatures in the upflow zones are elevated too. They are up to 200°C higher in the sedimentary basin and up to 100°C higher in the basement compared to the surrounding rocks (Figure 5). The difference between the temperature in the upflow zones and horizontal temperature average decreases with increasing depth (Figure 6). Over time, the temperature difference between the hot upflow zones and surrounding rocks of the basement tends to increase while the difference in flow rates decreases. The difference in temperature and flow rates between the upflow zones and surrounding rocks of the sedimentary basin, on the other hand, remains relatively constant but here the upflow zones migrate laterally over time. The flow rates in the basement are at least one order of magnitude lower

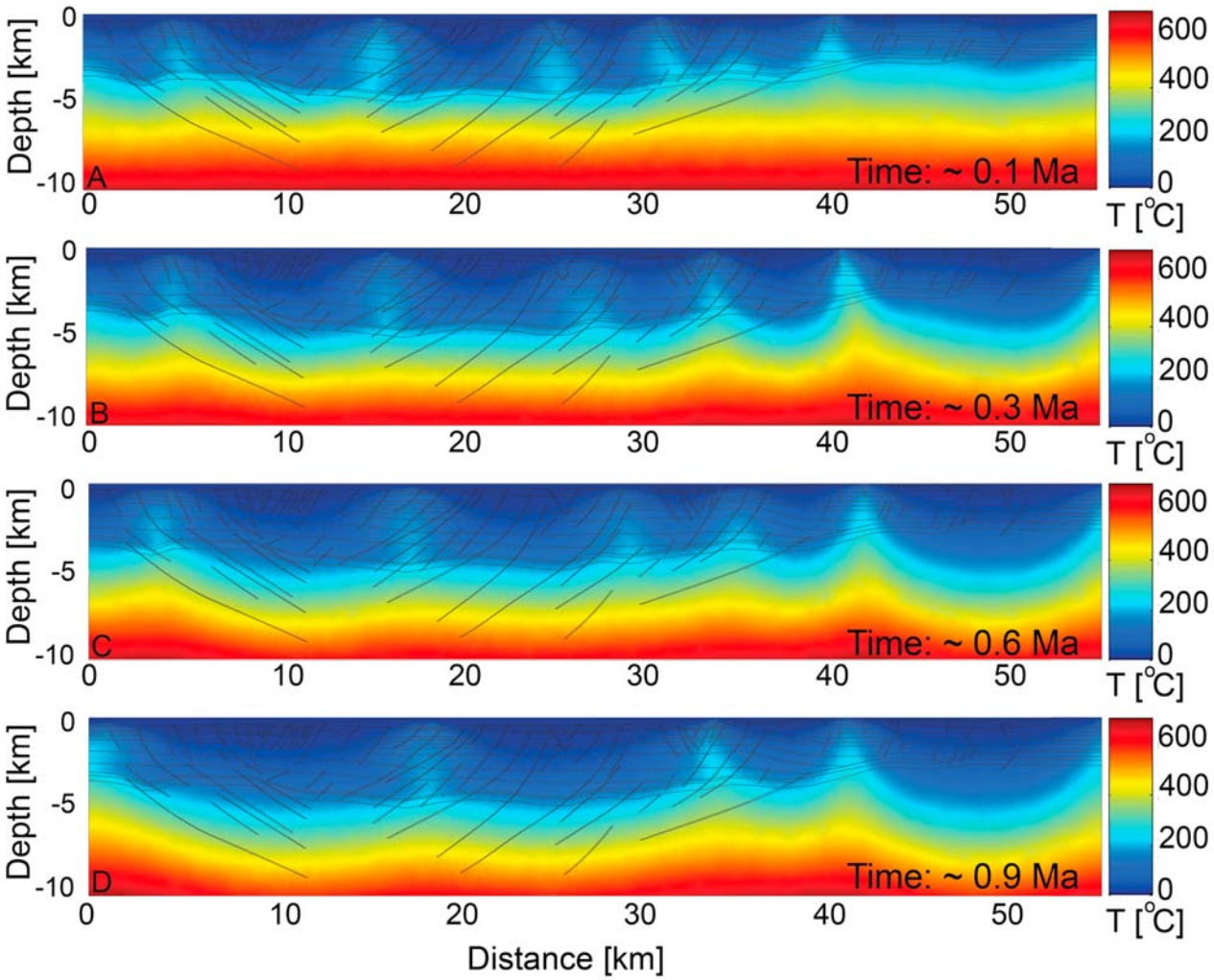

Figure 4. Evolution of the fluid temperatures in the TFZ at (a) ~0.1 Ma, (b) ~0.3 Ma, (c) ~0.6 Ma, and (d) ~0.9 Ma. The lines show the outlines of the faults, the crystalline basement, and the sedimentary layers. The basal heat flow is 0.18 W m^{-2}.

compared to the sedimentary basin, which emphasizes the two distinct flow domains.

[42] Fluid flow occurs mainly in a single fault in the fault clusters. However, flow can leave one fault and move to another, thereby bridging the less permeable host rocks (Figure 7a). This creates hydrothermal upflow zones that are wider than the individual faults. These flow patterns in the vicinity of fault clusters also suggest that "master faults", which we define here as major throughgoing faults that connect the deep basement with the sedimentary basin and focus large volumes of fluids, may not be present in the TFZ.

[43] The occurrence of the two separate flow systems is caused by the geological structure of the TFZ. Fluid flow in the sedimentary basins is dominated by advective transport because the high permeability sediments allow for convection to occur. However, in the crystalline basement, heat transport is dominated by conduction since the permeability is less than 10^{-16} m^2 [*Manning and Ingebritsen*, 1999]. Solute transport is driven by diffusion and advection in the sedimentary basins and in the crystalline basement. This is because the lowest permeability that we imposed at depth reaches 10^{-19} m^2, which is still higher than the lowest permeability above which solute advection can occur [*Manning and Ingebritsen*, 1999].

4.2. Sedimentary Basins

[44] The temperature distribution in the sedimentary layers is not homogeneous due to the occurrence of narrow upflow zones which separate large areas of cold fluids which percolate downward from the seafloor. They cool large parts of the basins by kilometer-scale convective circulation before mixing with the hot fluids rising from the top of the crystalline basement. Such strong convection was also inferred from seismic data by *Riedel et al.* [2005]. The upflow and downflow regions show different geothermal gradients and different Darcy velocities (Figures 4 and 5). In the sedimentary basins, the downwelling zones are characterized by

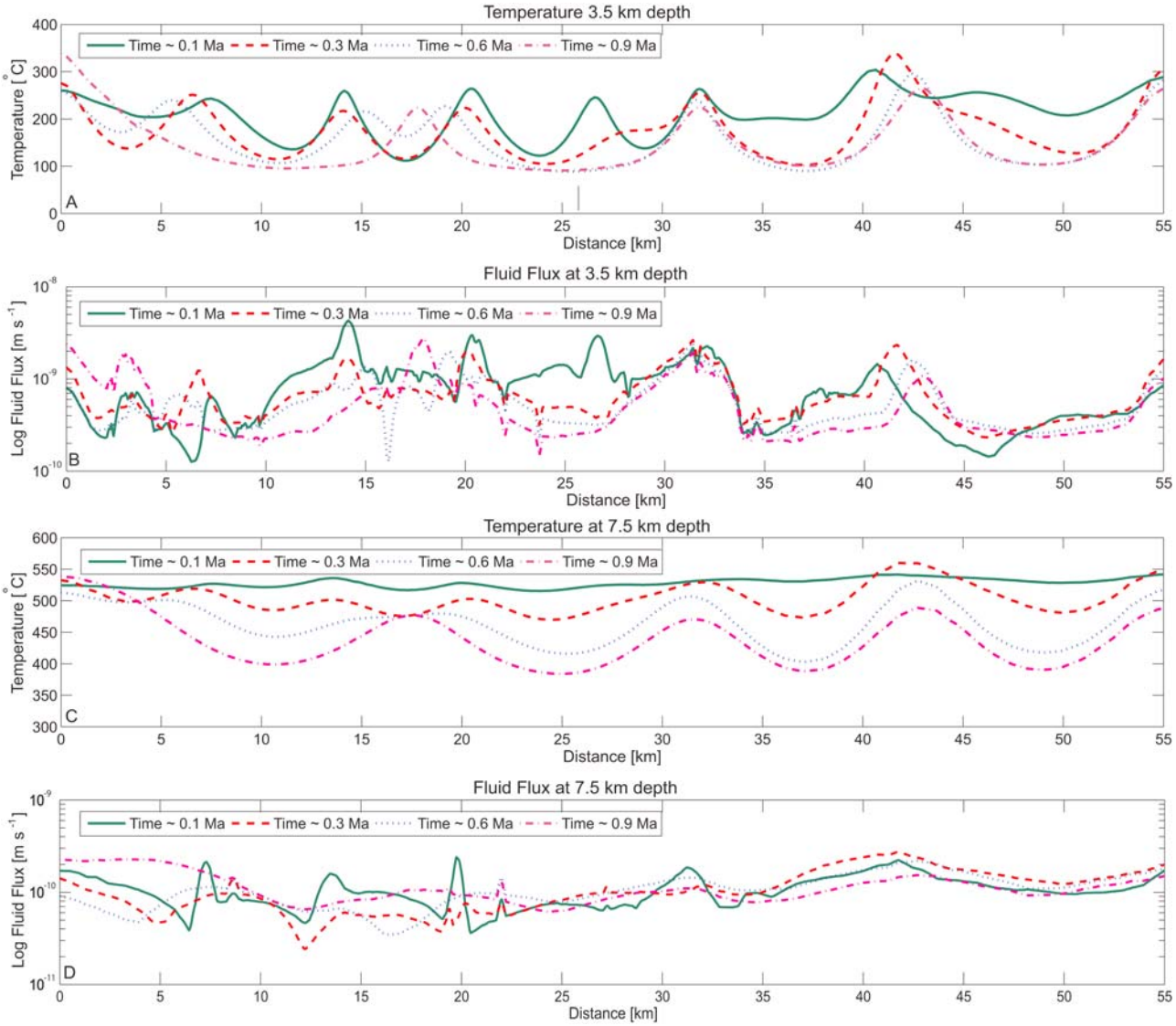

Figure 5. Horizontal cross sections of (a and c) temperatures and (b and d) flow rates at 3.5 km and 7.5 km depth and different times. The basal heat flow rate is 0.18 W m^{-2}. The fault-hosted upflow zones in the basement and sedimentary basin are characterized by elevated temperatures and flow rates.

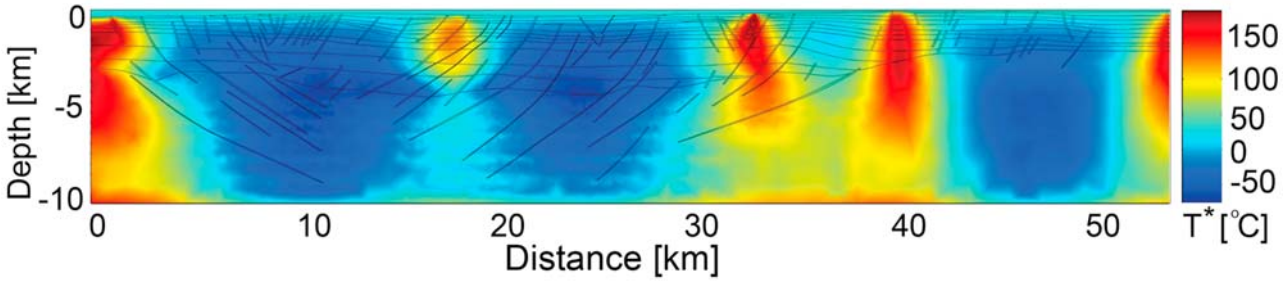

Figure 6. Temperature field after 0.9 Ma (see Figure 4d) with its lateral average removed. The reduced temperature, $T^{\star}$, is computed as $T^{\star}(x, z, t) = T(x, z, t) - \hat{T}$, where $\hat{T}$ is the horizontal temperature average given by $\hat{T}(z, t) = \frac{1}{x_{\max}} \int_0^{x_{\max}} T(x, z, t)dx$. Note that the horizontal stripes are an artefact, arising from calculating $\hat{T}$ on an unstructured finite element mesh with greatly varying element sizes.

temperatures ranging from 5°C to ~200°C. Hence large regions of the TFZ have an average geothermal gradient of ~40°C km^{-1}, which is low if we consider a heat flow rate at depth of 0.18 W m^{-2} but explains the low heat flow rates inferred by *Flóvenz and Sæmundsson* [1993].

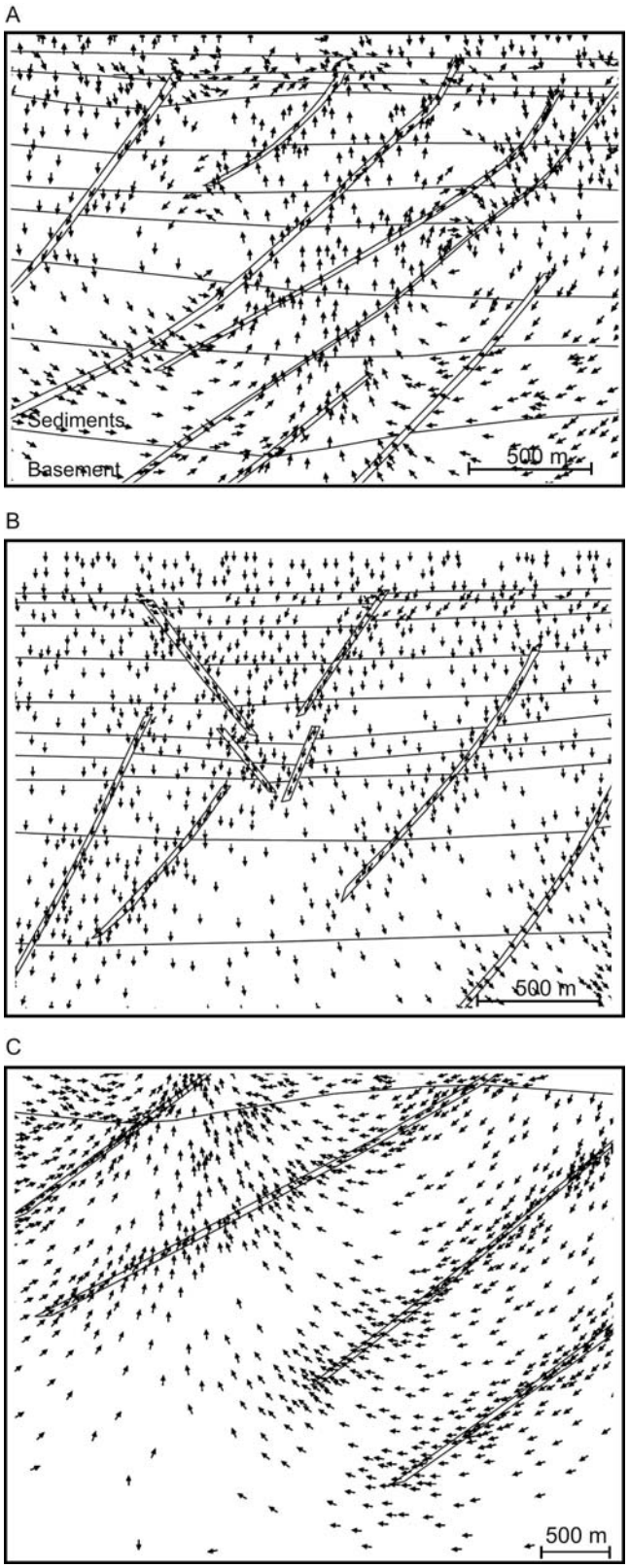

[45] Parts of the Húsavik Flatey Fault are exhumed on the Flateyjarskagi peninsula where the rocks have been uplifted by ~1.5 km [*Gudmundsson*, 1999]. Veins from these exhumed parts of the Húsavik Flatey Fault were probably not created by deep hydrothermal fluids but from relatively local and cold fluids that were driven downward and toward the faults by gravity [*Gudmundsson*, 1999]. Such flow patterns are also visible in our numerical simulations (Figure 7b). The downward motion proposed by *Gudmundsson* [1999] occurs in more than 90% of the area of our models. The remaining 10% are characterized by upflow zones where plumes of hot fluids migrate from the lower crust upwards through the sedimentary layers (Figure 4).

[46] The temperatures at the base of the upwelling plumes range between 300°C and 350°C. These are the highest fluid temperatures in the sedimentary basins. The temperatures of the uppermost parts of the upflow areas are in good agreement with the geological observations in the Húsavik region. The borehole Húsavik-Hola nr. 1 [*Tomasson et al.*, 1969], located at the east end of our geological model and approximately 1500 m away from the Húsavik Flatey Fault, shows temperatures of 105°C at depths of 1.2 km. Our simulations show that the temperature at the top part of the plumes is approximately 105°C at ~1.4 km depth, comparable to the borehole temperatures. Further evidence of shallow and isolated geothermal activity is the occurrence of a hot spring 100 m south of the Laugardalur fault [*Tomasson et al.*, 1969]. The Laugardalur fault runs on-land, parallel to the Húsavik Flatey Fault, and is located 1.5 km north of Húsavik. Moreover, a few warm springs in the Húsavik harbor indicate a geothermal anomaly near the town of Húsavik which we also observe in our numerical simulations.

[47] At the contact between the deepest sedimentary unit (sediment 13) and the top of the crystalline basement, strong lateral fluid flow occurs (Figure 7). This is due to the low permeability of the crystalline rocks which allows the percolation of only small volumes of fluids. Therefore the downwelling fluids are forced to flow laterally along the sediments basement contact before they merge with an upflow zone.

4.3. Basement

[48] In contrast to the relatively cold sedimentary basins, the temperatures of the crystalline basement range from ~200°C in the shallower parts to ~750°C in the deeper parts (Figure 4). The basement cools as the convective system in the overlaying sedimentary basin evolves (Figure 5). Although convection in the basement is less vigorous compared to the sedimentary basin and the difference in flow rates between

Figure 7. Closeups of the flow fields at selected locations in the two-dimensional geological model (Figure 2). (a) The convection patterns at the contact between sedimentary basin and crystalline basement in the vicinity of a cluster of faults (inset A in Figure 2). (b) The downward motion of fluids in the faults and sedimentary basin (inset B in Figure 2). (c) The migration of fluids from one fault to another in the crystalline basement (inset C in Figure 2). Note that the velocity vectors are not proportional to the flow rates and only a fraction of the actual velocity vectors is shown.

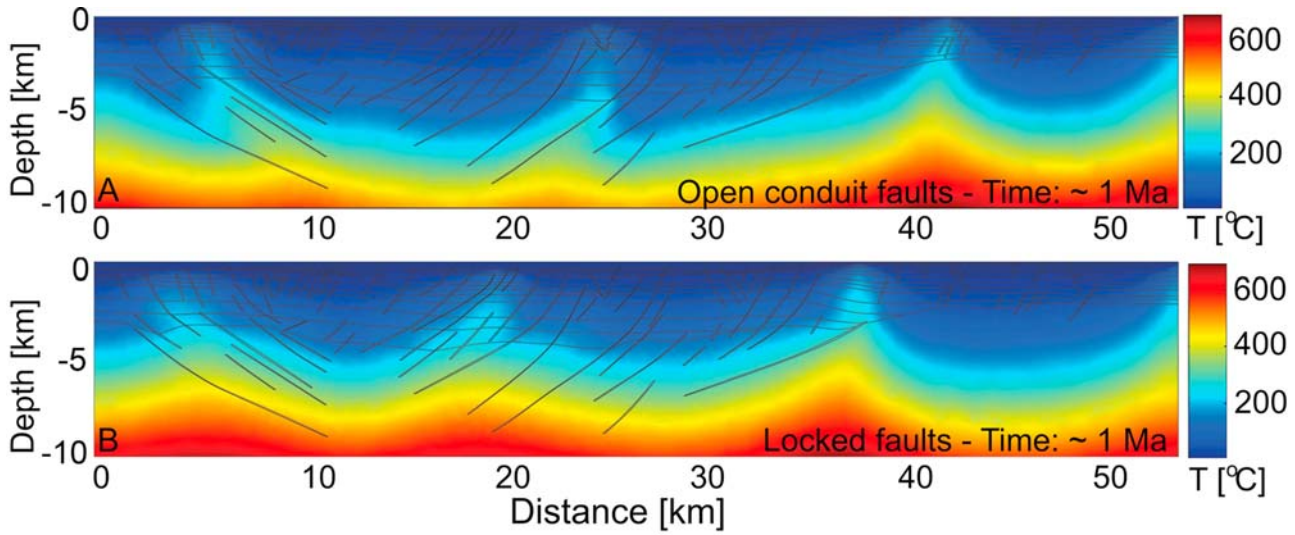

Figure 8. Temperature distributions after 1 Ma obtained applying the (a) "locked" and (b) "open conduit" setting. In the locked case the basement shows higher temperature and the "v-shaped" upflow pattern induced by the graben in the eastern part of the model is narrower. In the open conduit case the geothermal gradient in the basement is lower. Cold fluids of ~100 to 150°C can reach depths of up to 6 km.

upflow zones and surrounding rocks decreases with time, temperatures are elevated around the fault clusters that host the upflow zones and depressed below the large areas where fluids percolate downward in the sedimentary basin (Figures 4, 5, and 6). The downward fluid motion in the basement is influenced by plumes of rising, hot fluids in the sedimentary layers (Figure 7c). Below these areas, in the shallower parts of the crystalline basement, the upflow motion affects fluid advection over large distances. The effects are on a kilometer scale and depend on the structural features of the crust. Figure 7 shows how fluids leave the fault to flow upwards through the basement and contribute to the hot shallow plume.

5. Discussion

5.1. Relation to Geological Observations

[49] There is a considerable amount of geological data for the TFZ that gives insight into local flow phenomena. Our simulations help to put these observations into a coherent context. One key observation in our numerical results is the presence of isolated upflow regions in the TFZ which are surrounded by relatively large regions where cold fluids percolate downward. Isolated systems of upwelling hydrothermal fluids have been observed in the TFZ [*Tomasson et al.*, 1969; *Riedel et al.*, 2001] and even include hot hydrocarbon bearing fluids rising from deep sources [*Geptner et al.*, 2006]. The juxtaposition of warm upwelling fluids and large areas of cold downwelling fluids causes strong lateral variations in geothermal gradients. This may explain at least partly the variations in heat flow measurements reported for the TFZ [*Palmason*, 1974; *Flóvenz et al.*, 1985; *Flóvenz and Sæmundsson*, 1993; *Fridleifsson*, 1994; *Flóvenz*, 2008] and confirms the cold fluids which are thought to have formed the vein patterns around the Húsavik Flatey Fault [*Gudmundsson*, 1999].

[50] A key limitation is that our model is based on a two-dimensional geometry because a three-dimensional model with the same level of geological detail would have been computationally too intensive. Hence we cannot account for the effects of regional groundwater flow on convection or for convection of fluids in the fault plane itself, which often occurs in hydrothermal systems [*Bächler et al.*, 2003]. It is therefore likely that the hot upwelling areas are not aligned with our cross section but are more widespread in the TFZ. However, this still agrees well with the isolated occurrence of hot upwelling fluids discovered in the TFZ and our two-dimensional model still provides a physically realistic explanation for their occurrence.

5.2. Influence of the Faults

[51] The faults play a crucial role in controlling the large-scale and small-scale fluid flow in the TFZ. Most notably, the upflow regions are located in areas where clusters of faults occur and seem not to be associated with "master faults" which connect the upper sedimentary basins with the basement and could hence link the two distinct flow systems. It is important to reiterate that the location and extent of the faults has been interpreted from the seismic line. The concept of upflow zones centering around fault clusters may hence partly be due to the interpretation of the seismic section; wider faults (or additional large faults) may change this picture but would also require a reinterpretation of the seismic cross section and a revision of the geological model which we did not attempt.

[52] We ran additional simulations to analyze the influence of the fault permeability on fluid flow using two different scenarios, "locked" and "open conduit" faults. In the first case, the shallow part of the faults have a constant permeability of 10^{-16} m^2, while the deep parts have a depth dependent permeability and are less permeable than the crystalline basement by 2 orders of magnitude. In the second

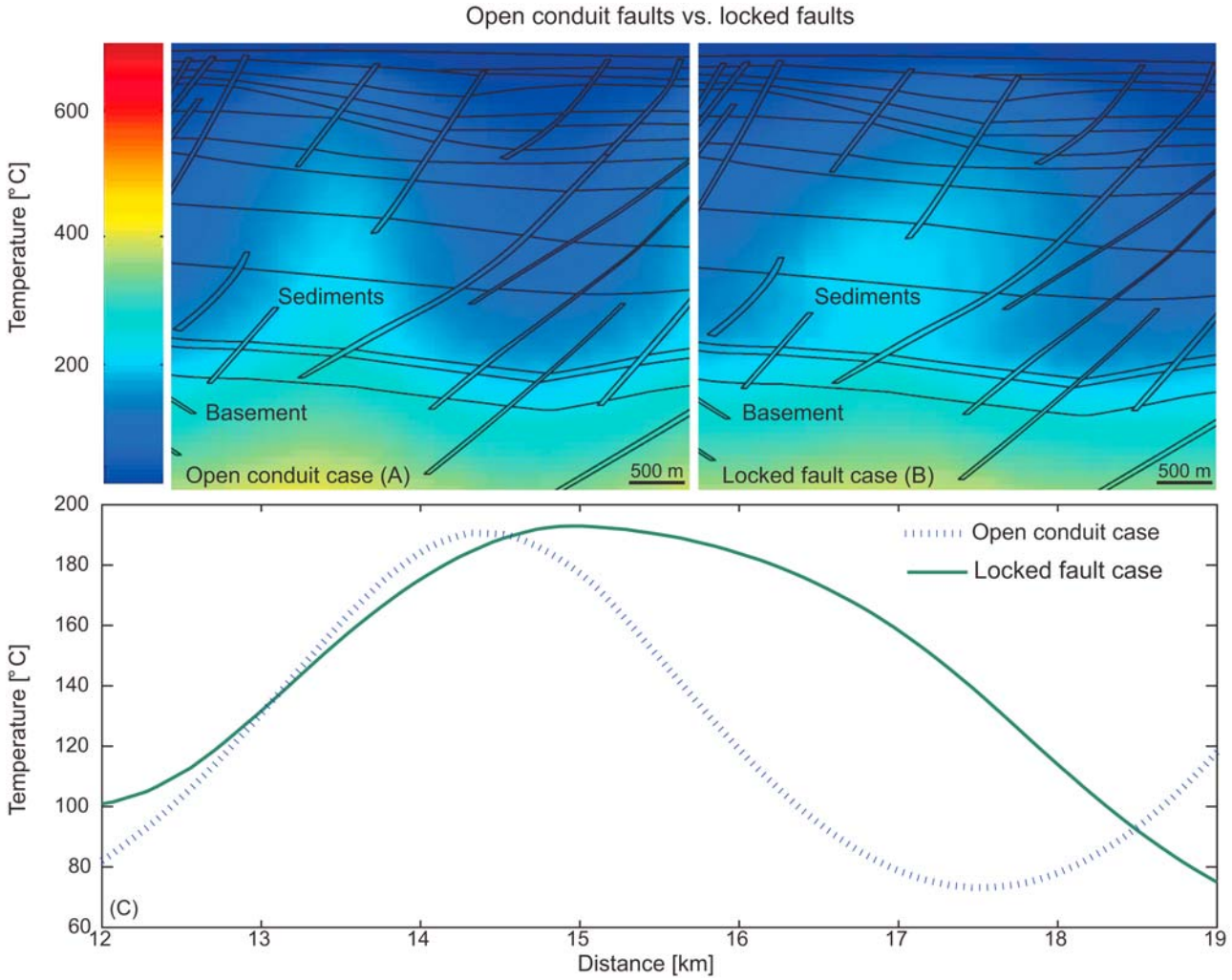

Figure 9. Comparison between the shape of the upflow zones in the (a) "locked" and (b) "open conduit" case. (c) The plumes in the locked case show a colder base just above the basement and are wider in the central part, as is visible in the temperature profile taken horizontally across the structure. The lines show the outlines of the faults and sedimentary layers.

case, both the shallow and the deep parts of the faults have a constant permeability of 10^{-14} m^2.

[53] Figure 8 shows the comparison between the temperature distributions obtained applying the locked and open conduit settings. There are distinct differences in the resulting temperature patterns but also variations from the temperature distributions obtained for the fault permeabilities listed in Table 1 (Figure 8). The "v-shaped" upflow pattern induced by the graben located in the eastern part of our model is wider in the open conduit case and the westernmost upflow area does not occur in the same location. In the open conduit case, the crystalline basement is characterized by lower temperatures at depth; between ~100 and 150°C at 6 km. The shape of the upflow zones is different for the locked and the open conduit scenarios (Figure 9). While both settings show that hot upflow zones still originate at the top of the basement, their shape and location depend on the permeability of the faults (Figure 9). The upflow zones in the locked case are characterized by a narrow base just above the basement. Here the fluids have temperatures of ~200°C and the width of the upflow zones increases toward its central part where fluid temperatures are between 125°C and 175°C. Fluid flow is not focused into the faults and instead the faults act as barriers to flow. Fluids flow in between these barriers through the sedimentary basin. With this setting we observe upflow zones up to 6 km wide. Yet, the overall pattern is not affected by the presence of low-permeability faults and the two separate flow systems still occur. However, low-permeability faults throughout the TFZ are less probable because of the extensional tectonic setting of this region where most of these faults are thought to be still active (B. Richter, personal communication, 2007). Hence the low-permeability, i.e., locked fault, case is less likely.

[54] If the fault permeability in the open conduit case is increased even further to 10^{-13} m^2, the rising hydrothermal fluids reach 300°C and separate into a brine and vapor phase at shallow depths (less than 300 m depth). The basement cools down strongly in the vicinity of some faults and can reach locally temperatures of 300°C at 8 km depth. These permeabilities lead to the occurrence of high flow rates and to the dynamic formation of a brine and vapor

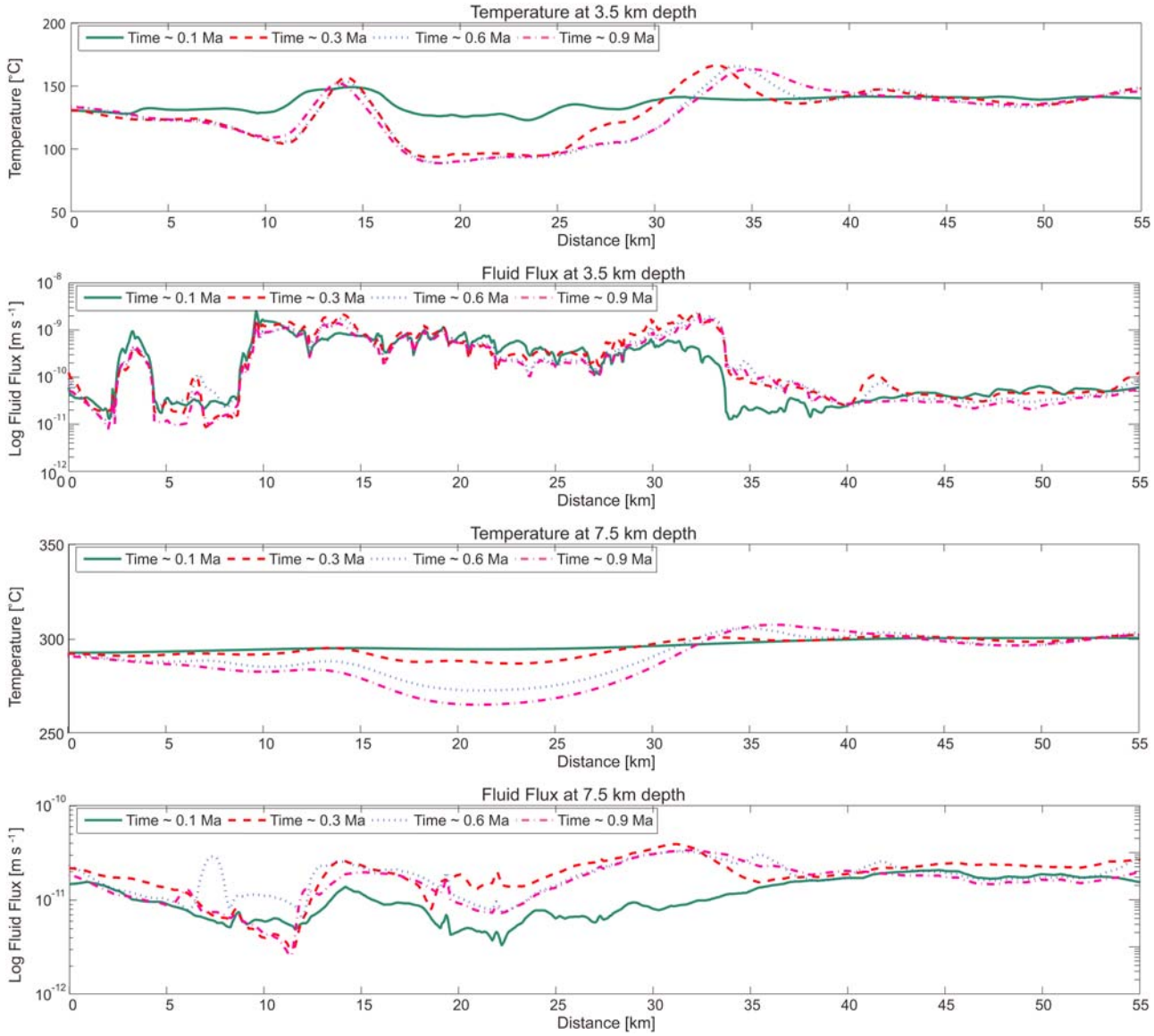

Figure 10. Horizontal cross sections of (a and c) temperatures and (b and d) flow rates at 3.5 km and 7.5 km depth and different times. The basal heat flow rate is 0.1 W m^{-2}. Compared to the heat flow rate of 0.18 W m^{-2} (Figure 5), the fault-hosted upflow zones in the sedimentary basin are less pronounced and essentially absent in the basement.

phase. The width of the upflow zones in this case is narrower, up to 2 km wide, as observed in other hydrothermal systems where faults are thought to have a similarly high permeability [*Heft et al.*, 2008]. The maximum Darcy velocities of ~1 m s^{-1} for this setting have the same magnitude as the velocities predicted by for another off-axis seafloor hydrothermal system, the Lau Basin in Australia [*Schardt et al.*, 2006]. In this case the flow rates are significantly higher than the flow rates typically predicted for a mid-ocean ridge system [*Coumou et al.*, 2008]. However, to the best of our knowledge, geological data of the TFZ do not show mid-ocean ridge like behavior, with high fluid temperatures and boiling at shallow depths. Also, it is probably unlikely that faults at 10 km depth have such high permeabilities, at least for extended periods. Hence we favor a model where the permeability contrast in the crystalline basement between crust and faults is not large, perhaps a factor 2 to 5, and where at least some of the shallow faults in the sedimentary basin are 10 to 50 times more permeable than the sedimentary rocks.

5.3. Influence of the Heat Flow

[55] We ran additional simulations with a basal heat flow of 0.1 W m^{-2} and 0.15 W m^{-2} to analyze the influence of different heat flow rates on fluid flow. A heat flow of 0.1 W m^{-2} results in a relatively homogeneous geothermal gradient of ~55°C km^{-1}. Although such a geothermal gradient agrees well with the data from *Flóvenz et al.* [1985], large convection cells or isolated upflow zones are far less pronounced in the sedimentary basins and essentially absent in the basement (Figure 10). In contrast to the strong lateral variations in temperature observed along horizontal cross

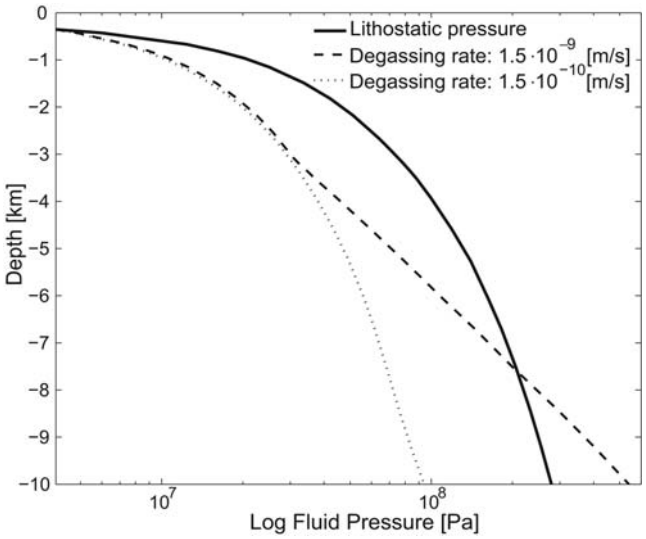

Figure 11. Fluid and lithostatic pressure as a function of depth and mantle degassing rates. Fluid pressures above hydrostatic can occur due to moderate mantle degassing rates. Since no degassing rates are available for the TFZ, we assumed a value of 1.5×10^{-9} m s^{-1}, similar to the average degassing rate proposed by *Fridriksson et al.* [2006] for south Iceland.

sections for the high heat flow rates (Figure 5), the same cross sections for a heat flow rate of 0.1 W m^{-2} show only small lateral changes in temperature (Figure 10). The elevated temperatures are not clearly correlated to elevated flow rates, although the flow rates vary laterally over two orders of magnitude in the sedimentary basin and one order of magnitude in the basement (Figure 10). Due to the absence of a large-scale convection system, the separation into two distinct flow systems is also missing. At a heat flow rate of 0.15 W m^{-2}, convection occurs in the sedimentary basins and in the crystalline basement but the presence of two isolated flow systems is still less pronounced. Since there is geological evidence for large-scale convection in the TFZ [*Riedel et al.*, 2005], we favor a high heat flow rate of 0.18 W m^{-2}.

5.4. Possible Relation Between Large-Scale Fluid Flow and the Seismic Events

[56] A key aim of our study was to provide insight into the proposed link between hydrodynamics and seismicity in the TFZ. The most pertinent feature that emerges in our simulations is the formation of two separate flow systems: one in the sedimentary basins, comprising more vigorous convection, and one in the crystalline basement, dominated by conduction. Fluid exchange between the two systems is limited due to a moderate permeability contrast at the basin-basement interface and a restricted number of upflow zones that connect basement and sedimentary basins. Based on seismic data, such a flow system was also proposed for the TFZ by *Riedel et al.* [2005] and by *Geoffroy and Dorbath* [2008] for the Reykjanes Peninsula in the south of Iceland. *Geoffroy and Dorbath* [2008] speculated that two flow systems are separated at approximately 2 to 3 km depth by an impermeable barrier. They can communicate when the impermeable barrier is breached during a large-magnitude earthquake. Our simulations show that the formation of two distinct flow domains is in fact very likely and a direct consequence of a relatively small permeability contrast between basement and sedimentary basin. At least for the TFZ a continuous impermeable layer is not necessary to create these two domains, which may be relatively common in hydrothermal systems. If the flow system is disturbed during a seismic event such that the two fluid reservoirs begin to communicate, mixing of shallow and deep fluids is probable. This was proposed for the TFZ by *Claesson et al.* [2004, 2007] who provided hydrogeochemical evidence of deep fluids rising to 1 km depth near the town of Húsavik immediately after a 5.8 M earthquake which occurred in September 2002 in the TFZ.

[57] Recent research has demonstrated that fluids driven by overpressure can migrate along faults at great speed due to the sudden enhancement of permeability caused by the dynamic changes in effective stress during seismic events [*Miller et al.*, 2004; *Sibson*, 2007]. Data for the TFZ suggest that the fluid pressure in the crystalline basement can be above hydrostatic, possibly close to lithostatic [*Crampin et al.*, 2002; *Stefansson et al.*, 2008]. Such excess pore pressure can be readily explained by accounting for a relatively small mantle degassing rate of 1.5×10^{-9} m s^{-1} for Iceland [*Fridriksson et al.*, 2006] which causes an increase in fluid pressures in the basement (Figure 11). The dehydration of altered (hydrate) mafic basement during burial could also cause such elevated fluid pressure in the crystalline basement. We hence suggest that our simulations represent the initially stable "interseismic" state in the TFZ (Figure 12a). Coseismic permeability changes away from the earthquake epicenter have recently been demonstrated [*Elkhoury et al.*, 2006] and we suggest that such a mechanism enhances the permeability of a fault (Figure 12b). The areas of permeability enhancement and decay, that is the location where a toggle switch mechanism occurs, are probably in the vicinity of the fault-hosted upflow zones, or below them in case of large-magnitude earthquakes which occur at greater depth. The faults in the upflow zones are already partially open and probably mechanically weak. Pulses of overpressured fluids from the crystalline basement can move upwards along these faults during coseismic permeability enhancement, temporarily changing the fluid temperature and chemistry in the sedimentary basins as observed by *Claesson et al.* [2004, 2007]. Notably, our numerical simulations as well as geological observations suggest an upflow zone of hot hydrothermal fluids in the vicinity of Húsavik. We have observed flow rates of up to 1 m s^{-1} for high permeability faults ($k = 10^{-13}$ m^2) even in the absence of an overpressured basement. This implies that basement fluids can readily be transported over kilometer distances in a few hours. As the pressure dissipates, the fault permeability begins to decrease and the fluid pressure in the basement begins to build up, completing the toggle switch cycle [*Miller and Nur*, 2000].

[58] An important prerequisite for this toggle switch mechanism in the TFZ is that the permeability of the deep faults is sufficiently low to foster the buildup of excess pressure in the basement and limit hydraulic communication between the sedimentary basin and crystalline basement. At the same time the fault permeability must also be higher

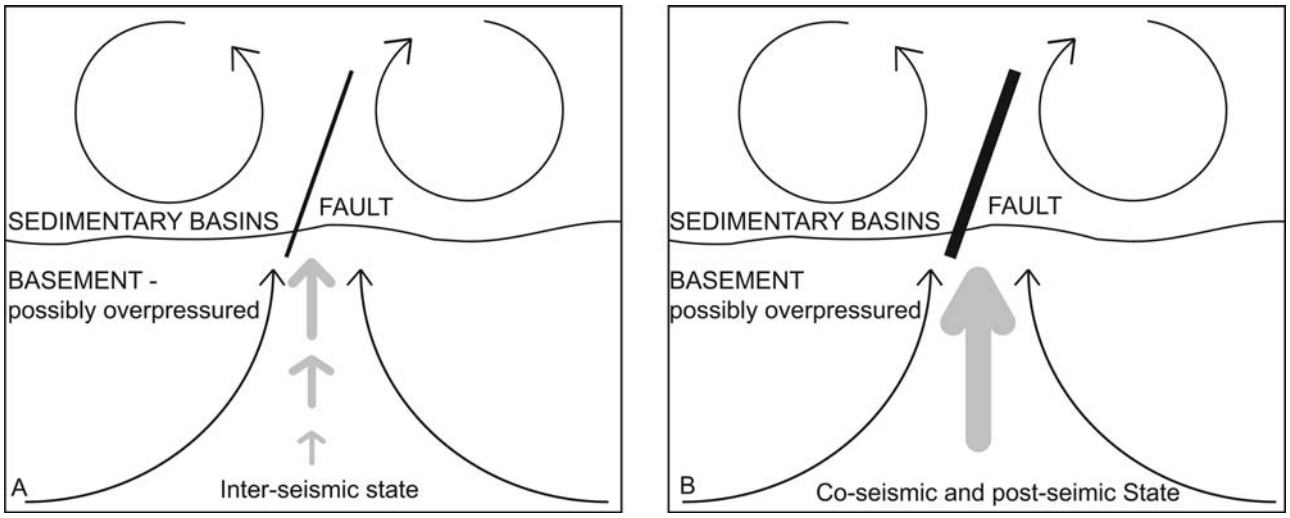

Figure 12. Idealized sketch showing the (a) "interseismic" and (b) coseismic and immediate postseismic states of the crust. The curved arrows depict the two flow systems in the sedimentary basins and in the crystalline basement, respectively. The black line represents an idealized fault. Its thickness is proportional to its permeability. The vertical arrows show the fluids upwelling from the basement. Coseismic permeability increase, and a possibly overpressured basement, lead to rapid and short-lived fluid escape from the basement in the already existing upflow zones.

than the average permeability of the basement to allow the formation of fault-hosted upflow zones. Our simulations suggest that fault permeabilities 2 to 5 times higher than the basement permeability create the right conditions for the toggle switch mechanism to occur.

[59] While our model can explain the coseismic and immediate postseismic changes in hydrogeochemistry and switching of fluid sources observed by *Claesson et al.* [2004, 2007], it does not offer a direct explanation as to why statistically significant changes in hydrogeochemistry at Húsavik have also been observed before the 5.8 M earthquake. *Claesson et al.* [2004, 2007] attribute these preseismic variations to stress-induced local changes in permeability and subsequent leakage of deeper fluids, which were in equilibrium with hot basalt, into shallower crustal sections. This hypothesis is still inline with our model because the buildup of excess pressure in the basement may well lead to a local enhancement of permeability shortly before the seismic event, probably in the vicinity of the fault-hosted upflow zones where fluid flow is being focused and the crust is already weakened. A detailed modeling effort, outwith the scope of this paper, would be required to study the effects of preseismic variations in fault permeability as the stress field changes.

6. Conclusions

[60] We have simulated the regional fluid flow in the Tjörnes Fracture Zone using a high-resolution model based on geological and geophysical data and physically realistic thermodynamic properties for hydrothermal fluids. Such simulations are now computationally possible and allow us to study the emergent behavior of a particular hydrothermal system while also accounting for the geological structures observed in nature. From this we can draw the following three conclusions for the Tjörnes Fracture Zone.

[61] Our simulations show that most fluids in the sedimentary basins are comparatively cold because large areas of the shallow crust are dominated by fluids that percolate downward from the seafloor. Only 10% of the sedimentary basins are characterized by hot plumes of deep origin hydrothermal fluids which depart from the top of the crystalline basement and reach shallow depths. This explains the occurrence of isolated hydrothermal fields observed in the Tjörnes Fracture Zone.

[62] Faults play a key role in controlling the large-scale and small-scale fluid flow dynamics of the Tjörnes Fracture Zone and hence influence the temperature distribution. The location and the shape of the upflow areas is directly related to the permeability of the faults. Low permeability faults imply wide upflow areas at shallow depths while high permeability faults lead to narrower upflow areas. Since the spreading rate of the area is ~1 cm yr^{-1}, the occurrence of impermeable faults is unlikely. On the other hand, the simulations showed that high permeability faults cause phase separation at shallow depths which has not been reported for the Tjörnes Fracture Zone. We hence suggest that the deeper parts of the faults have a permeability that is slightly higher than the permeability of the surrounding basement rocks while the shallower parts have a permeability 10 to 50 times higher than the rocks comprising the sedimentary basin.

[63] The key feature that emerges from our simulation and links the hydrodynamics and seismicity in the TFZ is the presence of two separated flow systems: one occurring in the sedimentary basins and one in the crystalline basement. The first is characterized by vigorous fluid convection and a heterogeneous geothermal gradient, the second by a more uniform geothermal gradient and conduction. The two flow domains form as a consequence of a moderate permeability contrast at the basement-basin interface, which limits com-

munication between the two systems. This large-scale flow pattern is thought to represent the "interseismic" state between main seismic events. The initially stable interseismic flow regime can be disturbed locally by coseismic enhancement of the permeability of faulted crustal portions. This causes rapid mixing between the shallow and the deep flow system because overpressured fluids rise at rates of possibly up to 1 m s^{-1}. As the fault permeability decays due to mineral precipitation and increase in effective normal stress, the communication between the two flow regimes decreases. This toggle switch mechanism was suggested based on hydrogeochemical variations observed before and after an M 5.8 earthquake in the Tjörnes Fracture Zone near the town of Húsavik. Our simulations show that the hydrodynamic conditions in the Tjörnes Fracture Zone support this hypothesis and implies that the toggle switch mechanism might be effective in the vicinity of the fault-hosted upflow zones. Numerical and geological evidence suggest that such a zone exists close to Húsavik.

[64] **Acknowledgments.** We thank the Edinburgh Collaborative of Subsurface Science and Engineering, a joint research institute of the Edinburgh Research Partnership in Engineering and Mathematics, for supporting this work. We also thank Lillemor Claesson, Alasdair Skelton, Shaul Hurwitz, and Agust Gudmundsson for fruitful discussions. The help of Bjarne Richter in making data available to us is greatly appreciated. The manuscript benefitted greatly from the careful reviews and constructive comments by Arie van den Berg and Steve Ingebritsen. Ctirad Matyska and Patrick Taylor are thanked for the editorial handling.

References

Arnórsson, S. (1995a), Geothermal systems in Iceland: Structure and conceptual models I. High temperature areas, *Geothermics*, *24*(5–6), 561–602.

Arnórsson, S. (1995b), Geothermal systems in Iceland: Structure and conceptual models II. Low temperature areas, *Geothermics*, *24*(5–6), 603–629.

Bächler, D., T. Kohl, and L. Rybach (2003), Impact of graben-parallel faults on hydrothermal convection: Rhine graben case study, *Phys. Chem. Earth*, *28*(9–11), 431–441.

Bodvarsson, G. S., S. M. Benson, O. Sigurdsson, V. Stefansson, and E. T. Eliasson (1984a), The Krafla geothermal field, Iceland 1. Analysis of well test data, *Water Resour. Res.*, *20*(11), 1515–1530.

Bodvarsson, G. S., K. Pruess, V. Stefansson, and E. T. Eliasson (1984b), The Krafla geothermal field, Iceland 2. The natural state of the system, *Water Resour. Res.*, *20*(11), 1531–1544.

Bodvarsson, G. S., K. Pruess, V. Stefansson, and E. T. Eliasson (1984c), The Krafla geothermal field, Iceland 3. The generating capacity of the field, *Water Resour. Res.*, *20*(11), 1545–1559.

Cathles, L. M. (1977), An analysis of the cooling of intrusives by groundwater convection which includes boiling, *Econ. Geol.*, *72*(5), 804–826.

Claesson, L., A. Skelton, C. Graham, C. Dietl, C. M. Morth, P. Torssander, and I. Kockum (2004), Hydrogeochemical changes before and after a major earthquake, *Geology*, *32*(8), 641–644.

Claesson, L., A. Skelton, C. Graham, and C. M. Morth (2007), The timescale and mechanisms of fault sealing and water-rock interaction after an earthquake, *Geofluids*, *7*, 427–440.

Coumou, D., T. Driesner, and C. A. Heinrich (2008), The structure and dynamics of mid-ocean ridge hydrothermal systems, *Science*, *321* (5897), 1825–1828.

Coumou, D., T. Driesner, P. Weis, and C. A. Heinrich (2009), Phase separation, brine formation and salinity variation at black smoker hydrothermal systems, *J. Geophys. Res.*, *114*, B03212, doi:10.1029/2008JB005764.

Crampin, S., A. Gudmundsson, and R. Stefansson (2002), Indication of high pore-fluid pressures in a seismically-active fault zone, *Geophys. J. Int.*, *151*(2), 1–5.

Driesner, T. (2007), The system H_2O - NaCl. Part II. Correlations for molar volume, enthalpy, and isobaric heat capacity from 0 to 1000°C, 1 to 5000 bar, and 0 to 1 XNaCl, *Geochim. Cosmochim. Acta*, *71*(20), 4902–4919.

Driesner, T., and S. Geiger (2007), Numerical simulation of multiphase fluid flow in hydrothermal systems, *Rev. Mineral. Geochem.*, *65*(1), 187–212.

Driesner, T., and C. A. Heinrich (2007), The system H_2O - NaCl. Part I: Correlation formulae for phase relations in temperature–pressure–composition space from 0 to 1000°C, 0 to 5000 bar, and 0 to 1 XNaCl, *Geochim. Cosmochim. Acta*, *71*(20), 4880–4901.

Einarsson, P. (1976), Relative location of earthquakes in the Tjörnes fracture zone, *Soc. Sci. Iceland*, *5*, 45–60.

Elkhoury, J. E., E. E. Brodsky, and D. C. Agnew (2006), Seismic waves increase permeability, *Nature*, *441*, 1135–1138.

Evans, J. P., C. B. Forster, and J. V. Goddard (1997), Permeability of fault-related rocks, and implications for hydraulic structure of fault zones, *J. Struct. Geol.*, *19*(11), 1393–1404.

Fisher, A. T., et al. (2003), Hydrothermal recharge and discharge across 50 km guided by seamounts on a young ridge flank, *Nature*, *421*, 618–621.

Flóvenz, O. G. (2008), On geothermal energy in Iceland, paper presented at the 11th International Symposium on District Heating and Cooling, Nordic Energy Res., Reykjavik, Iceland.

Flóvenz, O. G., and K. Saemundsson (1993), Heat flow and geothermal processes in Iceland, *Tectonophysics*, *225*(1–2), 123–138.

Flóvenz, O. G., L. S. Georgsson, and K. Árnason (1985), Resistivity structure of the upper crust in Iceland, *J. Geophys. Res.*, *90*, 10,136–10,150.

Fontaine, F. J., W. S. D. Wilcock, and D. A. Butterfield (2007), Physical controls on the salinity of mid-ocean ridge hydrothermal vent fluids, *Earth Planet. Sci. Lett.*, *257*(1–2), 132–145.

Fridleifsson, G. O. (1994), Geothermal gradient and hydrothermal systems off north Iceland, *Rep. GF-94-05*, p. 4, Orkustofnun Natl. Energy Auth., Reykjavík.

Fridriksson, T., B. R. Kristjánsson, H. Ármannsson, E. Margrétardóttir, S. Ólafsdóttir, and G. Chiodini (2006), CO_2 emissions and heat flow through soil, fumaroles, and steam heated mud pools at the Reykjanes geothermal area, SW Iceland, *Appl. Geochem.*, *21*(9), 1551–1569.

Garven, G., S. W. Bull, and R. R. Large (2001), Hydrothermal fluid flow models of stratiform ore genesis in the McArthur basin, Northern territory, Australia, *Geofluids*, *1*, 289–311.

Geiger, S., S. Roberts, S. K. Matthäi, C. Zoppou, and A. Burri (2004), Combining finite element and finite volume methods for efficient multiphase flow simulations in highly heterogeneous and structurally complex geologic media, *Geofluids*, *4*, 284–299.

Geiger, S., T. Driesner, C. A. Heinrich, and S. K. Matthäi (2005), On the dynamics of H_2O - NaCl fluid convection in the Earth's crust, *J. Geophys. Res.*, *110*, B07101, doi:10.1029/2004JB003362.

Geiger, S., T. Driesner, C. A. Heinrich, and S. K. Matthäi (2006a), Multiphase thermohaline convection in the Earth's crust: I. A new finite element–finite volume solution technique combined with a new equation of state for H_2O - NaCl, *Transp. Porous Media*, *63*(3), 399–434.

Geiger, S., T. Driesner, C. A. Heinrich, and S. K. Matthäi (2006b), Multiphase thermohaline convection in the Earth's crust: II. Benchmarking and application of a finite element–finite volume solution technique with a H_2O - NaCl equation of state, *Transp. Porous Media*, *63*(3), 435–461.

Geoffroy, L., and C. Dorbath (2008), Deep downward fluid percolation driven by localized crust dilatation in Iceland, *Geophys. Res. Lett.*, *35*, L17302, doi:10.1029/2008GL034514.

Geptner, A. R., B. Richter, Y. I. Pikovskii, S. S. Chernyansky, and T. A. Alekseeva (2006), Hydrothermal polycyclic aromatic hydrocarbons in marine and lagoon sediments at the intersection between Tjörnes fracture zone and recent rift zone (Skjálfandi and Öxarfjördhur bays), Iceland, *Mar. Chem.*, *101*(3–4), 153–165.

Gudmundsson, A. (1999), Fluid overpressure and stress drop in fault zones, *Geophys. Res. Lett.*, *26*(1), 115–118.

Gudmundsson, A. (2001), Fluid overpressure and flow in fault zones: Field measurements and models, *Tectonophysics*, *336*(1–4), 183–197.

Gudmundsson, A. (2007), Infrastructure and evolution of ocean-ridge discontinuities in Iceland, *J. Geodyn.*, *43*(1), 6–29.

Gudmundsson, A., S. Brynjolfsson, and M. T. Jonsson (1993), Structural analysis of a transform fault-rift zone function in north Iceland, *Tectonophysics*, *220*(1–4), 205–221.

Gunnarsson, K. (1998), Sedimentary basins of the N-Iceland shelf: Draft version for discussion, *Rep. OS-98014*, Orkustofnun Natl. Energy Auth., Reykjavík.

Hanson, R. B. (1995), The hydrodynamics of contact metamorphism, *Geol. Soc. Am. Bull.*, *107*(5), 595–611.

Hayba, D. O., and S. E. Ingebritsen (1997), Multiphase groundwater flow near cooling plutons, *J. Geophys. Res.*, *102*, 12,235–12,252.

Heft, K. L., K. M. Gillis, M. A. Pollock, J. A. Karson, and E. M. Klein (2008), Role of upwelling hydrothermal fluids in the development of alteration patterns at fast spreading ridges: Evidence from the sheeted dike

complex at Pito deep, *Geochem. Geophys. Geosyst.*, *9*(5), Q05O07, doi:10.1029/2007GC001926.
Hensch, M., C. Riedel, J. Reinhardt, and T. Dahm (2007), Hypocenter migration of fluid-induced earthquake swarms in the Tjörnes fracture zone (north Iceland), *Tectonophysics*, *447*(1–4), 80–94.
Hill, D. P., et al. (1993), Seismicity remotely triggered by the magnitude 7.3 landers, California, earthquake, *Science*, *260*(5114), 1617–1623.
Hurwitz, S., K. L. Kipp, S. E. Ingebritsen, and M. E. Reid (2003), Groundwater flow, heat transport, and water table position within volcanic edifices: Implications for volcanic processes in the Cascade Range, *J. Geophys. Res.*, *108*(B12), 2557, doi:10.1029/2003JB002565.
Husen, S., R. Taylor, R. B. Smith, and H. Healser (2004), Changes in geyser eruption behavior and remotely triggered seismicity in Yellowstone national park produced by the 2002 7.9M Denali fault earthquake, Alaska, *Geology*, *32*(6), 537–540.
Ingebritsen, S. E., and W. E. Sanford (2006), *Groundwater in Geologic Processes*, Cambridge Univ. Press, Cambridge, U. K.
Ingebritsen, S. E., S. Geiger, S. Hurwitz, and T. Driesner (2010), Numerical simultion of magmatic hydrothermal systems, *Rev. Geophys.*, *48*, RG1002, doi:10.1029/2009RG000287.
Jakobsdóttir, S. S., G. B. Gudmundsson, and R. Stefansson (2002), Seismicity in Iceland 1991–2000 monitored by the SIL seismic system. *Jokülll*, *51*, 87–94.
Jóhannesson, H., and K. Saemundsson (1998), Geological map of Iceland, scale 1: 500 000, Tectonics Icelandic Inst. of Nat. History, Reykjavík.
Johnson, H. P., M. Hutnak, R. P. Dziak, C. G. Fox, I. Urcuyo, J. P. Cowen, J. Nabelek, and C. Fisher (2000), Earthquake-induced changes in a hydrothermal system on the Juan de Fuca mid-ocean ridge, *Nature*, *407*, 174–177.
Join, J. L., J. L. Folio, and B. Robineau (2005), Aquifers and groundwater within active shield volcanoes: Evolution of conceptual models in the Piton de la Fournaise volcano, *J. Volcanol. Geotherm. Res.*, *147*(1–2), 187–201.
Lowell, R. P. (1991), Modeling continental and submarine hydrothermal systems, *Rev. Geophys.*, *29*, 457–476.
Lowell, R. P., S. R. Gosnell, and Y. Yang (2007), Numerical simulations of single-pass hydrothermal convection at mid-ocean ridges: Effects of the extrusive layer and temperature-dependent permeability, *Geochem. Geophys. Geosyst.*, *8*, Q10011, doi:10.1029/2007GC001653.
Manga, M., and E. Brodsky (2006), Seismic triggering of eruptions in the far field: Volcanoes and geysers, *Annu. Rev. Earth Planet. Sci.*, *34*, 263–291.
Manning, C. E., and S. E. Ingebritsen (1999), Permeability of the continental crust: Implications of geothermal data and metamorphic systems, *Rev. Geophys.*, *37*(1), 127–150.
Matthäi, S. K., C. A. Heinrich, and T. Driesner (2004), Is the mount Isa copper deposit the product of forced brine convection in the footwall of a major reverse fault?, *Geology*, *32*(4), 357–360.
Matthäi, S. K., S. Geiger, S. G. Roberts, A. Paluszny, M. Belayneh, A. Burri, A. Mezentsev, H. Lu, D. Coumou, and T. Driesner (2007), Numerical simulation of multi-phase fluid flow in structurally complex reservoirs, *Geol. Soc. Spec. Publ.*, *292*(1), 405–429.
Miller, S. A., and A. Nur (2000), Permeability as a toggle switch in fluid-controlled crustal processes, *Earth Planet. Sci. Lett.*, *183*(1–2), 133–146.
Miller, S. A., C. Collettini, L. Chiaraluce, M. Cocco, M. Barchi, and B. J. P. Kaus (2004), Aftershocks driven by a high-pressure CO_2 source at depth, *Nature*, *427*, 724–727.
Palmason, G. (1974), Heat flow and hydrothermal activity in Iceland, in *Geodynamics of Iceland and the North Atlantic Area*, edited by L. Kristjansson, pp. 297–306, D. Reidel, Dordrecht, Netherlands.
Palmason, G., and K. Saemundsson (1974), Iceland in relation to the mid-atlantic ridge, *Annu. Rev. Earth Planet. Sci.*, *2*(1), 25–50.
Paluszny, A., S. K. Matthäi, and M. Hohmeyer (2007), Hybrid finite element-finite volume discretization of complex geologic structures and a new simulation workflow demonstrated on fractured rocks, *Geofluids*, *7*, 186–208.
Riedel, C., M. Schmidt, R. Botz, and F. Theilen (2001), The grimsey hydrothermal field offshore north Iceland: Crustal structure, faulting and related gas venting, *Earth Planet. Sci. Lett.*, *193*(3–4), 409–421.
Riedel, C., A. Tryggvason, T. Dahm, R. Stefanson, R. Bödvarson, and G. B. Gudmundsson (2005), The seismic velocity structure north of Iceland from joint inversion of local earthquake data, *J. Seismol.*, *9*(4), 383–404.
Roeloffs, E., M. Sneed, D. L. Galloway, M. L. Sorey, C. D. Farrar, J. F. Howle, and J. Hughes (2003), Water-level changes induced by local and distant earthquakes at Long Valley caldera, California, *J. Volcanol. Geotherm. Res.*, *127*(3–4), 269–303.
Rögnvaldasson, S. T., A. Gudmundsson, and R. Slunga (1998), Seismotectonic analysis of the Tjörnes Fracture Zone, an active transform fault in north Iceland, *J. Geophys. Res.*, *103*30,117–30,129.
Saemundsson, K. (1974), Evolution of the axial rifting zone in northern Iceland and the Tjörnes fracture zone, *Geol. Soc. Am. Bull.*, *85*(4), 495–504.
Saemundsson, K. (1979), Outline of the geology of Iceland, *Jokülll*, *29*, 7–28.
Schardt, C., R. Large, and J. Yang (2006), Controls on heat flow, fluid migration, and massive sulfide formation of an off-axis hydrothermal system–the Lau basin perspective, *Am. J. Sci.*, *306*(2), 103–134.
Sibson, R. H. (2007), An episode of fault-valve behavior during compressional inversion? The 2004 6. 8M mid - Niigata prefecture, Japan, earthquake sequence, *Earth Planet. Sci. Lett.*, *257*(1–2), 188–199.
Stefansson, R., G. B. Gudmundsson, and P. Halldorsson (2008), Tjörnes fracture zone: New and old seismic evidences for the link between the north Iceland rift zone and the mid-Atlantic ridge, *Tectonophysics*, *447*(1–4), 117–126.
Stüben, K. (2001), A review of algebraic multigrid, *J. Comput. Appl. Math.*, *128*, 281–309.
Sykes, L. R. (1967), Mechanism of earthquakes and nature of faulting on the mid-oceanic ridges, *J. Geophys. Res.*, *72*, 2131–2153.
Tomasson, J., G. Palmason, J. Jonsson, and S. Bjornsson (1969), Jardhiti vid Húsavik: Lithological report from the Icelandic energy association, 83 pp., Orkustofnun Natl. Energy Auth., Reykjavík.
Tryggvason, E. (1973), Seismicity, earthquake swarms, and plate boundaries in the Iceland region, *Bull. Seismol. Soc. Am.*, *63*(4), 1327–1348.
Wilcock, W. S. D. (1998), Cellular convection models of mid-ocean ridge hydrothermal circulation and the temperatures of black smoker fluids, *J. Geophys. Res.*, *103*, 2585–2596.

S. Geiger and M. Lupi, Institute of Petroleum Engineering, Heriot-Watt University, Edinburgh, EH14 4AS, UK. (sebastian.geiger@pet.hw.ac.uk; matteo.lupi@gmail.com)
C. M. Graham, School of Geosciences, Grant Institute, University of Edinburgh, Edinburgh, EH9 3JW, UK. (colin.graham@ed.ac.uk)